KSUPT – 10/1 March 2010

Constraining dark energy with gamma-ray bursts

Lado Samushia[1,2] and Bharat Ratra[1]

ABSTRACT

We use the measurement of gamma-ray burst (GRB) distances to constrain dark energy cosmological model parameters. We employ two methods for analyzing GRB data — fitting luminosity relation of GRBs in each cosmology and using distance measures computed from binned GRB data. Current GRB data alone cannot tightly constrain cosmological parameters and allow for a wide range of dark energy models.

Subject headings: cosmological parameters — distance scale — large-scale structure of universe — GRB

1. Introduction

The combination of recent measurements of distant supernovae Type Ia (SNe Ia) apparent magnitudes (Sahni et al. 2008; Cunha 2009; Perivolaropoulos & Shafieloo 2009; Hicken et al. 2009), cosmic microwave background anisotropy (Dunkley et al. 2009; Komatsu et al. 2009), the baryon acoustic signal in the power spectrum of galaxies (Eisenstein et al. 2005; Cole et al. 2005; Percival et al. 2007; Samushia & Ratra 2009a), and galaxy cluster gas mass fractions (Allen et al. 2008; Samushia & Ratra 2008; Ettori et al. 2009) indicates at high confidence that about 70% of the energy budget of the universe comes from non-luminous dark energy that is close to spatially uniform and has negative pressure.[1]

[1]Department of Physics, Kansas State University, 116 Cardwell Hall, Manhattan, KS 66506, USA lado@phys.ksu.edu, ratra@phys.ksu.edu.

[2]National Abastumani Astrophysical Observatory, Ilia State University, 2A Kazbegi Ave, GE-0160 Tbilisi, Georgia.

[1]This assumes that Einstein's general relativity provides an accurate description of gravitation on cosmological scales. Attempts to do away with dark energy by modifying general relativity are discussed by Hellwing & Juszkiewicz (2009), Sen & Devi (2010), Shaposhnikov & Zenhäusern (2009), Setare & Saridakis (2009), Harko (2008), Capozziello et al. (2008), Bamba et al. (2009), Aluri et al. (2009), and references therein. For a recent review see Silvestri & Trodden (2009).

Although the existence of dark energy is now a well-established observational fact its physical nature is still a topic of great debate. The simplest and historically first physical model of dark energy is the cosmological constant Λ that has an equation of state $p = -\rho$, where p is its pressure and ρ the energy density (Peebles 1984). The cosmological constant is introduced by hand into the equations of general relativity but could be related to the energy of the fluctuating vacuum. This ΛCDM model, although simple and in good accord with most available cosmological data[2] (e.g., Frieman et al. 2008), has a number of theoretical shortcomings (e.g., Ratra & Vogeley 2008). These include the so-called "smallness" and "coincidence" problems. The measured value of the cosmological constant energy scale is of order 10^{-3}eV, some 30 orders of magnitude smaller than the Planck scale, perhaps what we would expect the vacuum energy scale to be based on simple quantum field theoretical arguments. In addition, since the energy density of nonrelativistic matter is decreasing with the expansion of the Universe while the energy density of a cosmological constant is constant, there is a very narrow window in time when both of these have comparable energy densities, and it is unclear why we happen to live at this special time.

Because of these and other issues a number of different dark energy models have been considered. Typically these introduce a new component that acts like a cosmological constant, in that it is close to spatially homogeneous, while gradually decreasing in time to the small currently observed value. An early example of this class of models is the ϕCDM model in which dark energy is taken to be a scalar field ϕ (Peebles & Ratra 1988; Ratra & Peebles 1988). In this model, the current cosmological constant energy scale is small because the Universe is old. For recent reviews of dark energy see Caldwell & Kamionkowski (2009), Frieman (2009), and Sami (2009).[3]

Although available cosmological data can constrain dark energy models, they are not yet good enough to strongly discriminate between different dark energy models (see, e.g., Gong et al. 2009, Kilbinger et al. 2009, Coc et al 2009, and references therein). In the near future better-quality and more independent cosmological observations should be able to break this degeneracy (see, e.g., Wang et al. 2009; Mortonson et al. 2009; Thomas et al.

[2]The ΛCDM model assumes the cold dark matter (CDM) model of structure formation which might have some observational inconsistencies (see, e.g., Peebles & Ratra 2003; Perivolaropoulos 2009; Primack 2009, and references therein).

[3]In the ϕCDM model, we consider in this paper the dark energy scalar field couples to the matter only through gravity. For dark energy models with less restrictive couplings see Wang & Zhang (2008), Dent et al. (2009), La Vacca et al. (2009), Jamil (2009), Chongchitnan (2009), Nesseris (2009), and references therein. For other dark energy models see Bilić et al. (2009), Basilakos & Perivolaropoulos (2008), Grande et al. (2009), Dutta & Scherrer (2009), Feng (2009), Andrianov et al. (2010), and references therein.

2009; Arun et al. 2009; Yashar et al. 2009).[4]

SNe Ia were one of the first cosmological probes to give direct evidence for dark energy. These are very bright exploding stars and are standardizable candles that can be seen to very large distances. More then 300 well-calibrated distant SNe Ia have already been observed up to the redshift of 1.6 (Kowalski et al. 2008; Hicken et al. 2009). These measurements alone give more then 5σ evidence for the existence of dark energy, but they are not very effective in constraining dark energy model parameters overall unless used in combination with other data. Even when current SNe Ia data are combined with all other currently available data sets, we cannot yet determine if the energy density of dark energy is constant as required by the ΛCDM model or if it varies in time as suggested by dynamical alternatives such as ϕCDM. A dedicated SNe Ia space mission should result in significantly more higher quality data that should help resolve this issue (see, e.g., Podariu et al. 2001a; Alam et al 2009, and references therein.).

One way of improving our understanding of how dark energy behaves is to study the evolution of the universe at redshifts higher than those probed by SNe Ia. This requires standard candles that are visible at great distances. Gamma-ray bursts (GRBs) could in principle serve as such high redshift standardizable candles. They are the most luminous events in the universe today and can be seen beyond $z = 8$ (see, e.g., Tanvir et al. 2009).[5] If it is definitely established that GRBs are standardizable candles, their visibility at high-redshift should prove to be very useful in discriminating between ΛCDM and time-varying dark energy models.[6]

With the intention of getting cosmological constraints from GRB observations a number of GRB calibrations have been used so far (see, e.g., Schaefer 2007, and references therein).

---

[4]In the near future, measurements of nonlinear structure formation will help discriminate between different dark energy models, see, e.g., Grossi & Springel (2009), Francis et al. (2008), Casarini et al. (2009), and references therein. Other tests that hold significant potential are the angular size of radio sources and galaxies as a function of redshift (e.g., Daly et al. 2009; Santos & Lima 2008, and references therein) and measurement of the Hubble parameter as a function of redshift (e.g., Samushia & Ratra 2006; Lin et al. 2008; Dev et al. 2008; Fernandez-Martinez & Verde 2008, and references therein).

[5]For a review of GRB physics see, e.g., Mészáros (2006).

[6]For early discussions of the use of GRBs as a cosmology probe see, e.g., Lamb & Reichart (2000), Nemiroff (2000), Ghirlanda et al. (2004), Friedman & Bloom (2005), Firmani et al. (2005), Xu et al. (2005), Mörtsell & Sollerman (2005), Di Girolamo et al. (2005), Bertolami & Silva (2006), and Lamb et al. (2005). More recent studies may be traced back through Mosquera Cuesta et al. (2008), Amati et al. (2008), Basilakos & Perivolaropoulos (2008), Capozziello & Izzo (2008), Tsutsui et al. (2009), and Qi et al (2008).

One that gives least scatter and therefore most information is

$$\log\left(\frac{E_\gamma}{1\ \mathrm{erg}}\right) = A_1 + B_1 \log\left(\frac{E_{\mathrm{peak}}(1+z)}{300\ \mathrm{keV}}\right), \tag{1}$$

a relation that connects the total burst energy of the GRB (E_γ) to the peak energy of the GRB spectrum (E_{peak}) (Ghirlanda et al. 2004). Regrettably, we do not yet have a model-independent way of computing the coefficients A_1 and B_1. A better understanding of physical processes that result in the burst, or observations of nearby GRBs (to which distances can be measured independently), could in principle help us to calibrate the E_γ-E_{peak} relation without any prior assumptions. To extract cosmological information, GRBs have to be recalibrated for every dark energy model considered (at each set of parameter values). This is time consuming and also results in large statistical uncertainties and hence GRB cosmological constraints that are poor.

Recently, methods of calibrating GRBs in cosmology-independent manners have been proposed and used to constrain some dark energy models (see e.g., Kodama et al. 2008; Liang et al. 2008; Wei & Zhang 2008; Liang & Zhang 2008, that use SNe Ia measurements to externally calibrated GRBs). The resulting cosmological constraints are still loose, but in the future when more high precision GRB observations become available this could provide a strong test of dark energy.

Wang (2008) recently used data of 69 GRBs (Schaefer 2007) to construct a distance measure that can be used to constrain cosmological models. The advantage of this method is that internally calibrated GRB data may be straightforwardly combined with other data when deriving cosmological constraints. On the other hand, with this method the resulting cosmological results are sensitive to the chosen binning. This method also requires an input cosmological model and thus is not completely cosmology independent. When this method is used to constrain ΛCDM the GRB data favor lower values of both cosmological constant energy density (Ω_Λ) and nonrelativistic matter energy density (Ω_{m}) than do the SNe Ia data. The GRB data by themselves are unable to strongly constrain cosmological parameters, for example in spatially flat ΛCDM the GRB data require $\Omega_{\mathrm{m}} = 0.25^{+0.12}_{-0.11}$ at 1σ confidence (Wang 2008).

In this paper we use GRB data to constrain time variation of dark energy's energy density. First we recalibrate GRBs for each cosmological model and compare the result with the ones derived using the data and method of Wang (2008). We consider a ϕCDM model where a scalar field which is close to spatially uniform on cosmological scales slowly rolls down an almost flat potential and plays the role of dark energy.

In the next section, we summarize the dynamics of this scalar field dark energy model.

In Section 3, we describe our methods and computations. We present and discuss our results in Section 4.

2. Scalar field as dark energy

In the ϕCDM model, consistent with the indications from cosmic microwave background anisotropy measurements (e.g., Podariu et al. 2001b; Page et al. 2003), we only consider the spatially flat universe case. The invariant four-interval in a homogeneous and isotropic version of such a universe is

$$ds^2 = -dt^2 + a^2(t)d\vec{x} \cdot d\vec{x}, \tag{2}$$

where t is cosmic time, $d\vec{x}$ is the spatial separation in three-dimensional Euclidean space and $a(t)$ is the time-dependent scale factor which determines the change in distance between two distant noninteracting test particles in the universe.

In the set of models we consider the scalar field ϕ with Lagrangian density

$$\mathcal{L} = \frac{1}{2}\partial_\mu\phi\partial^\mu\phi - \frac{1}{2}V(\phi) \tag{3}$$

is the dark energy. Here $V(\phi)$ is the potential energy density of the scalar field. In the expanding, spatially homogeneous and isotropic universe described in Equation (2) the spatially homogeneous scalar field obeys the modified Klein-Gordon equation,

$$\ddot{\phi} + 3\frac{\dot{a}}{a}\dot{\phi} + \frac{1}{2}\frac{\partial V(\phi)}{\partial\phi} = 0, \tag{4}$$

and the dynamics of the scale factor is governed by

$$\left(\frac{\dot{a}}{a}\right)^2 = \frac{8\pi G}{3}(\rho_{\rm m} + \rho_\phi). \tag{5}$$

In Equation (5), G is the universal gravitational constant, and $\rho_{\rm m}$ and ρ_ϕ are the energy densities of nonrelativistic matter and the scalar field, respectively. If the scalar field is uniform in space then, from Equation (3), the energy density of the scalar field is

$$\rho_\phi = \frac{1}{32\pi G}\left(\dot{\phi}^2 + V(\phi)\right). \tag{6}$$

Since an underlying more fundamental explanation of dark energy remains elusive, there is as yet no first principles way of choosing the scalar field potential. If we choose the

potential energy density to be inversely proportional to a power of the scalar field, $V(\phi) \sim \phi^{-\alpha}$, the ϕCDM model has a number of very interesting features (Peebles & Ratra 1988; Ratra & Peebles 1988). First, even if the scalar field starts off from a very high energy density state, its energy density decreases to a very small value during the course of cosmic evolution. Second, in the radiation and matter-dominated epochs the evolution of the scalar field "tracks" the evolution of the dominant component. The scalar field slowly comes to dominate, leading to the end of matter domination and the start of the scalar field-dominated epoch. So, in the ϕCDM scenario the "smallness" and "coincidence" problems mentioned above are partially resolved because of the time-evolution properties of the scalar field. Even if the scalar field potential is not exactly inverse power law, this form of potential provides a very economic way of parameterizing the slowly-evolving dark energy scenario with just one positive parameter α. Moreover, unlike the XCDM parameterization of dark energy, the ϕCDM model is physically consistent (see, e.g., Ratra 1991).

In the ϕCDM model, the dark energy density, unlike the cosmological constant, varies slowly in time. The dark energy density increases as we go back in time and larger values of α correspond to faster evolution of dark energy. As a result, observable quantities such as luminosity and angular diameter distances in the ϕCDM model differ from the predictions of the ΛCDM model with a time-independent cosmological constant. Some predictions, of course, depend also on the values of other cosmological parameters, such as the Hubble constant H_0 or the energy density of baryonic matter $\Omega_{\rm b}$, and so many independent cosmological tests are required to break this degeneracy and constrain dark energy model parameters.

A number of cosmological tests have been used to constrain the ϕCDM model, including the angular sizes of radio sources and quasars as a function of redshift (Chen & Ratra 2003; Podariu et al. 2003; Daly et al. 2009), the apparent magnitude of SNe Ia as a function of redshift (Wilson et al. 2006; Samushia & Ratra 2009b), and the gas mass fraction of large relaxed clusters as a function of redshift (Chen & Ratra 2004; Samushia & Ratra 2008). Current cosmological observations are in good agreement with a time-independent cosmological constant in a close to spatially flat ΛCDM model, but slowly rolling scalar field dark energy in the ϕCDM model is not yet ruled out at high confidence.

In this paper we use measured GRB luminosity distance as a function of redshift to constrain slowly rolling scalar field and other dark energy models. Because of the calibration problems mentioned above, GRB data alone cannot constrain cosmological parameters effectively. We also combine the results obtained from the GRB analysis with constraints from SNe Ia and baryon acoustic peak measurements, to illustrate the effect and weight of current GRB data in such a combined analysis.

3. Cosmological constraints from GRB

Besides the $E_{\rm peak}$–E_γ relation, (Equation (1)), Schaefer (2007) uses four other calibrations for GRBs that relate total luminosity to directly measurable quantities. These calibration relations are given by

$$\begin{aligned}
\log\left(\frac{L}{1\mathrm{ergs}^{-1}}\right) &= A_2 + B_2 \log\left(\frac{\tau_{\rm lag}(1+z)^{-1}}{0.1\ \mathrm{s}}\right), \\
\log\left(\frac{L}{1\mathrm{ergs}^{-1}}\right) &= A_3 + B_3 \log\left(\frac{V(1+z)}{0.02}\right), \\
\log\left(\frac{L}{1\mathrm{ergs}^{-1}}\right) &= A_4 + B_4 \log\left(\frac{E_{\rm peak}(1+z)}{300\mathrm{KeV}}\right), \\
\log\left(\frac{L}{1\mathrm{ergs}^{-1}}\right) &= A_5 + B_5 \log\left(\frac{\tau_{\rm RT}(1+z)^{-1}}{0.01\mathrm{s}}\right),
\end{aligned} \tag{7}$$

where L is the absolute luminosity, $\tau_{\rm lag}$ is the GRB lag time (the time shift between the hard and soft curves), V is the variability (the normalized variance of an observed light curve around the smoothed light curve), $E_{\rm peak}$ is the peak energy of the GRB, and $\tau_{\rm RT}$ is the rise time or the time over which the light curve rises by half of the peak flux.

Following Schaefer (2007) we take Equations (7) and (1) and for each cosmological model find the best-fit values for the A and B parameters using the bisector least-square method (for a description see Isobe et al. 1990). We use the best-fit A and B values and the measured $\tau_{\rm lag}$, V, $E_{\rm peak}$, $\tau_{\rm RT}$ values to compute L and E_γ using the same Equations (7) and (1). For each calibration relation we then compute the luminosity distance as

$$\begin{aligned}
d_{\rm L}^2 &= \frac{L}{4\pi P_{\rm bolo}}, \\
d_{\rm L}^2 &= \frac{E_\gamma(1+z)}{4\pi S_{\rm bolo} F_{\rm beam}},
\end{aligned} \tag{8}$$

where $P_{\rm bolo}$ is the bolometric peak flux and $S_{\rm bolo}$ is the bolometric fluence of the GRB. $F_{\rm beam}$ is so-called beam factor $F_{\rm beam} = 1 - \cos\theta_{\rm jet}$, where $\theta_{\rm jet}$ is a jet opening angle.

We then derive an effective luminosity distance by weighting the five estimates of GRB luminosity distances,

$$\log(\bar{d}_L^2(z_i)) = \frac{\sum_\alpha \log(\bar{d}_L^2(z_i)_\alpha)/\sigma_{i,\alpha}^2}{\sum_\alpha 1/\sigma_{i,\alpha}^2}, \tag{9}$$

$$\sigma^2(\log(\bar{d}_L^2(z_i))) = 1/\sum_\alpha 1/\sigma_{i,\alpha}^2, \tag{10}$$

where index i runs over 69 redshift bins, and α over five calibration relations. To constrain cosmological parameters we use χ^2 defined by

$$\chi^2 = \sum_{\rm i=1}^{69} \frac{(\log(\bar{d}_L^2(z_i))^{\rm obs} - \log(\bar{d}_L^2(z_i))^{\rm th})^2}{\sigma^2(\log(\bar{d}_L^2(z_i))}. \tag{11}$$

We also adopt the method of Wang (2008) for using GRB data to constrain cosmological parameters. She placed each of the 69 GRBs in the redshift range $z = 0.17$ to $z = 6.6$ (Schaefer 2007) at a luminosity distance that minimized a combined χ^2 that took weighted account of all five calibration relations. She then computed a distance measure

$$\bar{r}_{\rm p} = \frac{r_{\rm p}(z)}{r_{\rm p}(0.17)}, \tag{12}$$

where

$$r_{\rm p}(z) = \frac{H_0}{hc} \frac{1}{z(1+z)^{1/2}} d_L(z), \tag{13}$$

and $d_L(z)$ is the luminosity distance at redshift z, $h = H_0/(100 \text{ km s}^{-1} \text{ Mpc}^{-1})$, and c is the speed of light. The ratio in Equation (12) does not depend on the Hubble constant and does not require information about the absolute calibration of GRBs (which are unknown).

Wang (2008) computed the distance measure $\bar{r}_{\rm p}$ in six redshift bins $\bar{r}_{\rm p}(z_{\rm i})$, $i = 1, 2, \ldots 6$. The values of $\bar{r}_{\rm p}(z_{\rm i})$ are shown in Table II and the normalized covariance matrix is shown in Table III of Wang (2008). For currently viable cosmological models, these $\bar{r}_{\rm p}(z_{\rm i})$ are almost completely independent of the cosmological model and so provide a useful summary of current GRB data (Wang 2008). This information can be used to constrain any dark energy model and the resulting GRB data constraints can be straightforwardly combined with other constraints. In this approach, χ^2 is given by

$$\chi^2(\Omega_{\rm m}, p) = \Delta(z_{\rm i}) \sigma_{\rm i} (S^{-1})_{\rm ij} \sigma_{\rm j} \Delta(z_{\rm j}), \tag{14}$$

where

$$\Delta(z_{\rm i}) = \bar{r}_{\rm p}^{\rm data}(z_{\rm i}) - \bar{r}_{\rm p}^{\rm theory}(z_{\rm i}), \tag{15}$$

$S_{\rm ij}$ is the normalized covariance matrix given in Table III of Wang (2008) and summation over repeated indexes is assumed. Here, $\sigma_{\rm i}$ is $\sigma_{\rm i}^+$ if $\Delta(z_{\rm i}) > 0$ and $\sigma_{\rm i}^-$ if $\Delta(z_{\rm i}) < 0$.

In this paper we consider three cosmological models, ΛCDM, the XCDM parameterization of the dark energy equation of state $p_{\rm x} = \omega_{\rm x} \rho_{\rm x}$ in a spatially flat universe, and the spatially flat ϕCDM model. Since we are comparing low-redshift predictions to observations we ignore the contribution of radiation in these models. In this case, in all three models, the background evolution can be fully described by two parameters, the fractional energy

density of nonrelativistic matter $\Omega_{\rm m}$ and a parameter p that describes the properties of dark energy. In ΛCDM p is the fractional energy density of the cosmological constant Ω_Λ, in XCDM it is the equation of state parameter $\omega_{\rm x}$, and in ϕCDM it is the positive parameter α that governs the steepness of the scalar field potential energy density.

In each model, for both methods, we divide the two-dimensional space of cosmological parameters into an equidistant grid, and for each pair of parameters $\Omega_{\rm m}$ and p we compute the theoretical luminosity distance. We then compute the difference between the theoretical prediction and the measured value at each of the 69 redshifts listed in Table 2 of Schaefer (2007) or the six redshifts listed in Table II of Wang (2008),

The best-fit parameters are defined as the pair $(\Omega_{\rm m}^*, p^*)$ that gives the minimum value of $\chi^2(\Omega_{\rm m}, p)$. The 1σ, 2σ, and 3σ confidence level contours are defined as the sets of points where the value of $\chi^2(\Omega_{\rm m}, p)$ is more than its minimum value $\chi^2(\Omega_{\rm m}^*, p^*)$ by 2.30, 6.18, and 11.83, respectively. If the likelihood function, $\propto \exp(-\chi^2/2)$, was Gaussian, the 3σ contour would be 99.7% likely to enclose the true values of cosmological parameters. In our case the likelihood function has a single maximum and decreases monotonically from the best-fit value point, so the true values of cosmological parameters are very unlikely to be outside the 3σ contours we compute.

Figures 1–6 show the constraints from the Wang (2008) GRB data on ΛCDM, XCDM, and ϕCDM model parameters. Figures 7–12 show the constraints derived using a method similar to that of Schaefer (2007).

4. Results and discussion

The GRB constraints shown in Figures 1–3 are consistent with the "standard" spatially flat $\Omega_\Lambda = 0.7$ ΛCDM model at a little under 2σ, with the GRBs mildly favoring a somewhat lower value of $\Omega_{\rm m}$ than the "standard" value that is compensated by space curvature and $\Omega_\Lambda = 0$ (Figure 1) or a mildly time-varying dark energy (Figures 2 and 3). While the constraints of Figs. 1–3 derived from the Wang (2008) data have not previously been shown, these results are implicit in the discussions of Wang (2008) and other analyses of GRB constraints, including Kodama et al. (2008), Liang & Zhang (2008), Amati et al. (2008), and Tsutsui et al. (2009).

These results, and the fact that the current GRB data contours are quite broad, are probably an indication of the preliminary nature of the current GRB data. Current GRB data by themselves are unable to effectively constrain cosmological parameters. The GRB constraints however, are a little tighter than radio galaxy angular size versus redshift constraints

(e.g., Daly et al. 2009), constraints from strong gravitational lensing data (e.g., Chae et al. 2004), and those from the measurement of the Hubble parameter as a function of redshift (e.g., Samushia et al. 2007).

To get tighter constraints on cosmological parameters, and to see how current GRB data affect constraints derived from other data sets, we combine the results of our GRB analysis with SNe Ia apparent magnitude versus redshift data (the Union data of Kowalski et al. 2008) and measurements of the baryon acoustic (BAO) peak (Percival et al. 2007). Since all three sets of measurements are independent, we define the total likelihood function of cosmological parameters for the combined data as a product of the individual likelihood functions,

$$\mathcal{L}_{\rm tot} = \mathcal{L}_{\rm GRB}\mathcal{L}_{\rm SN}\mathcal{L}_{\rm BAO}, \tag{16}$$

and compute the best-fit values and confidence level contours from $\mathcal{L}_{\rm tot}$ as before. The SNe Ia likelihood function $\mathcal{L}_{\rm SN}$ depends on the assumptions that we make about the value of the Hubble constant. Here we marginalize over $h = 0.73 \pm 0.03$ with the

4–6 show the constraints on cosmological parameters of the ΛCDM, XCDM, and ϕCDM models from a joint analysis of the SNe Ia Union and baryon acoustic peak measurements, without and with the GRB data. These plots show that current GRB data only marginally affect the joint SNeIa and BAO peak constraints (which are amongst the tightest provided by current data), favoring slightly lower values of the nonrelativistic matter density parameter $\Omega_{\rm m}$.

Figures 7–9 are similar to Figures 1–3, but derived by recalibrating GRB data for each cosmology, using a method similar to that of Schaefer (2007). The "standard" spatially flat $\Omega_\Lambda = 0.7$ ΛCDM model is about 2.5σ from the best-fit value. In all three models GRB data favor a nonrelativistic matter-dominated universe. Figures 10–12 show the joint constraints from GRB, SNe Ia and BAO data. The constraints are dominated by the SNe Ia and BAO data, with the GRB data shifting the best-fit values to slightly larger values of $\Omega_{\rm m}$.

The GRB constraints derived using the two different methods disagree with each other at more than 2σ confidence level (compare Figures 1–3 and 7–9). This is somewhat worrying but not completely unexpected as the field is still under rapid development.

GRB data alone do not provide tight constraints on cosmological parameters. Moreover, while not greatly significant, current GRB data favor cosmological parameter values that are at odds with what other data favor. When used in combination with some of the highest-quality current data (e.g., SNe Ia and BAO peak measurements) current GRB data only slightly change the results. This is mainly because in the absence of an absolute calibration

of GRBs they, as standard candles, have big measurement uncertainties. This is however quite likely to change as more and better-quality GRB measurements become available with improvements in methods to calibrate GRBs. GRBs could potentially provide a very strong test of the time variation of dark energy as they can be observed up to redshifts beyond eight, at distances where other standard candles cannot be detected.

We thank the referee for a detailed and helpful report. We acknowledge support from DOE grant DE-FG03-99EP41093 and the Georgian National Science Foundation grant ST08/4-442.

REFERENCES

Alam, U., Sahni, V., & Starobinsky, A. A. 2009, ApJ, 704, 1086

Allen, S. W., et al. 2008, MNRAS, 383, 879

Aluri, P. K., Jain, P., & Singh, N. K. 2009, Mod. Phys. Lett. A, 24, 1583

Amati, L., et al. 2008, MNRAS, 391, 577

Andrianov, A. A., Cannata, F., Kamenshchik, A. Y., & Regoli, D. 2010, Int. J. Mod. Phys. D., 19, 97

Arun, K. G., et al. 2009, Class. Quant. Grav. 26, 094021

Bamba, K., Geng, C.-Q., Nojiri, S., & Odintsov, S. D. 2009, Phys. Rev. D, 79, 083014

Basilakos, S., & Perivolaropoulos, L. 2008, MNRAS, 391, 411

Bertolami, O., & Silva, P. T. 2006, MNRAS, 365, 1149

Bilić, N., Tupper, G. A., & Viollier, R. D. 2009, Phys. Rev. D, 80, 023515

Caldwell, R. R., & Kamionkowski, M. 2009, Ann. Rev. Nucl. Part. Sci., 59, 397

Capozziello, S., Cianci, R., Stornaiolo, C., & Vignolo, S. 2008, Phys. Scr., 78, 065010

Capozziello, S., & Izzo, L. 2008, A&A, 490, 31

Casarini, L., Macciò, A. V., & Bonometto, S. A. 2009, J. Cosmology Astropart. Phys., 0903, 014

Chae, K.-H., Chen, G., Ratra, B., & Lee, D.-W. 2004, ApJ, 607, L71

Chen, G., & Ratra, B. 2003, ApJ, 582, 586

Chen, G., & Ratra, B. 2004, ApJ, 612, L1

Chongchitnan, S. 2009, Phys. Rev. D, 79, 043522

Coc, A., Olive, K. A., Uzan, J.-P., & Vangioni, E. 2009, Phys. Rev. D, 79, 103512

Cole, S., et al. 2005, MNRAS, 362, 505

Cunha, J. V. 2009, Phys. Rev. D, 79, 047301

Daly, R. A., et al. 2009, ApJ, 691, 1058

Dent, T., Stern, S., & Wetterich, C. 2009, J. Cosmology Astropart. Phys., 0901, 038

Dev, A., Jain, D., & Lohiya, D. 2008, arXiv:0804.3491 [astro-ph]

Di Girolamo, T., Catena, R., Vietri, M., & Di Sciascio, G. 2005, J. Cosmology Astropart. Phys., 0504, 008

Dunkley, J., et al. 2009, ApJS, 180, 306

Dutta, S., & Scherrer, R. J. 2008, Phys. Rev. D, 78, 123525

Eisenstein, D. J., et al. 2005, ApJ, 633, 560

Ettori, S., et al. 2009, å, 501, 61

Feng. C.-J. 2009, Phys. Lett. B, 672, 94

Fernandez-Martinez, E., & Verde, L. 2008, J. Cosmology Astropart. Phys., 0808, 023

Firmani, C., Ghisellini, G., Ghirlanda, G., & Avila-Reese, V., 2005, MNRAS, 360, L1

Francis, M. J., Lewis, C. F., & Linde, E. V. 2008, MNRAS, 393, L31

Friedman, A. S., & Bloom, J. S. 2005, ApJ, 627, 1

Frieman, J. A. 2009, arXiv:0904.1832 [astro-ph]

Frieman, J. A., Turner, M. S., & Huterer, D. 2008, ARA&A, 46, 385

Ghirlanda, G., Ghisellini, G., Lazzati, D., & Firmani, C. 2004, ApJ, 613, L13

Gong, Y., Zhang, T.-J., Lan, T., & Chen, X.-L. 2009, arXiv:0810.3572 [astro-ph]

Grande, J., Pelinson, A., & Solà, J. 2009, Phys. Rev. D, 79, 043006

Grossi, M., & Springel, V. 2009, arXiv:0809.3404 [astro-ph]

Harko, T. 2008, Phys. Lett. B, 669, 376

Hellwing, W. A. & Juszkiewicz, R. 2009, Phys. Rev. D, 80, 083522

Hicken, M. et al. 2009, ApJ, 700, 1097

Isobe, T., Feigelson, E. D., Akritas, M. G., & Babu, G. J. 1990, ApJ, 364, 104

Jamil, M. 2009, arXiv:0810.2896 [gr-qc]

Kilbinger, M., et al. 2009, A&A, 497, 677

Kodama, Y., et al. 2008, MNRAS, 391, L1

Komatsu, E., et al. 2009, ApJS, 180, 330

Kowalski, M., et al. 2008, ApJ, 686, 749

Lamb, D. Q. & Reichart, D. E. 2000, ApJ, 536, 1

Lamb, D. Q., et al. 2005, arXiv:astro-ph/0507362

La Vacca, G., Bonometto, S. A., & Colombo, L. P. L. 2009, New Astron. 14, 435

Liang, N., Xiao, W. K., Liu, Y., & Zhang, S. N. 2008, ApJ, 685, 354

Liang, N. & Zhang, L. N. 2008, AIP Conf. Proc., 1065, 367

Lin, H., Zhang, T.-J., & Yuan, Q. 2008, Mod. Phys. Lett. A, 24, 1699

Mészáros, P. 2006, Rep. Prog. Phys., 69, 2259

Mortonson, M. J., Hu, W., & Huterer, D. 2009, Phys. Rev. D, 79, 023004

Mörtsell, E., & Sollerman, J. 2005, J. Cosmology Astropart. Phys., 0506, 009

Mosquera Cuesta, H. J., Dumet, M., H., & Furlanetto, C. 2008, J. Cosmology Astropart. Phys., 0807, 004

Nemiroff, R. J. 2000, ApJ, 544, 805

Nesseris, S. 2009, Phys. Rev. D, 79, 044015

Page, L., et al. 2003, ApJS, 148, 233

Peebles, P. J. E. 1984, ApJ, 284, 439

Peebles, P. J. E., & Ratra, B. 1988, ApJ, 325, L17

Peebles, P. J. E., & Ratra, B. 2003, Rev. Mod. Phys., 75, 559

Percival, W. J., et al. 2007, MNRAS, 381, 1053

Perivolaropoulos, L. 2009, arXiv:0811.4684 [astro-ph]

Perivolaropoulos, L., & Shafieloo, A. 2009, Phys. Rev. D, 79, 123502

Podariu, S., Daly, R. A., Mory, M., & Ratra, B. 2003 ApJ, 584, 577

Podariu, S., Nugent, P., & Ratra, B. 2001a, ApJ, 553, 39

Podariu, S., Souradeep, T., Gott, J. R., Ratra, B., & Vogeley, M. S. 2001b, ApJ, 559, 9

Primack, J. R. 2009, arXiv:0902.2506 [astro-ph.CO]

Qi, S., Wang, F.-Y., & Lu, T. 2008, å, 487, 853

Ratra, B. 1991, Phys. Rev. D, 43, 3802

Ratra, B., & Peebles, P. J. E. 1988, Phys. Rev. D, 37, 3406

Ratra, B., & Vogeley, M. S. 2008, PASP, 120, 235

Sahni, V., Shafieloo, A., & Starobinsky, A. A. 2008, Phys. Rev. D, 78, 103502

Sami, M. 2009, Curr. Sci., 97 887

Samushia, L., Chen, G., & Ratra, B. 2007, arXiv:0706.1963 [astro-ph]

Samushia, L., & Ratra, B. 2006, ApJ, 650, L5

Samushia, L., & Ratra, B. 2008, ApJ, 680, L1

Samushia, L., & Ratra, B. 2009a, ApJ, 703, 1904

Samushia, L., & Ratra, B. 2009b, ApJ, 701, 1373

Santos, R. C., & Lima, J. A. S. 2008, Phys. Rev. D, 77, 083505

Schaefer, B. E. 2007, ApJ, 660, 16

Sen, A. A., & Devi, N. C. 2010, Gen. Rel. Grav., 42, 821

Setare, M. R., & Saridakis, E. N. 2009, Phys. Lett. B, 671, 331

Shaposhnikov, M., & Zenhäusern, D. 2009, Phys. Lett. B, 671, 87

Silvestri, A., & Trodden, M. 2009, Rep. Prog. Phys., 72, 096901

Tanvir, N. R., et al. 2009, Nature, 461, 1254

Thomas, S. A., Abdalla, F. B., & Weller, J. 2009, MNRAS, 395, 197

Tsutsui, R., et al. 2009, MNRAS, 394, L31

Wang, S., & Zhang, Y. 2008, Phys. Lett. B, 669, 201

Wang X., et al. 2009, MNRAS, 394, 1775

Wang, Y. 2008, Phys. Rev. D, 78, 123532

Wei, H., & Zhang, S. N. 2008, Eur. Phys. J. C., 63, 139

Wilson, K. M., Chen, G., & Ratra, B. 2006, Mod. Phys. Lett. A, 21, 2197

Xu, D., Dai, Z. G., & Liang, E. W. 2005, ApJ, 633, 603

Yashar, M., et al. 2009, Phys. Rev. D, 79, 103004

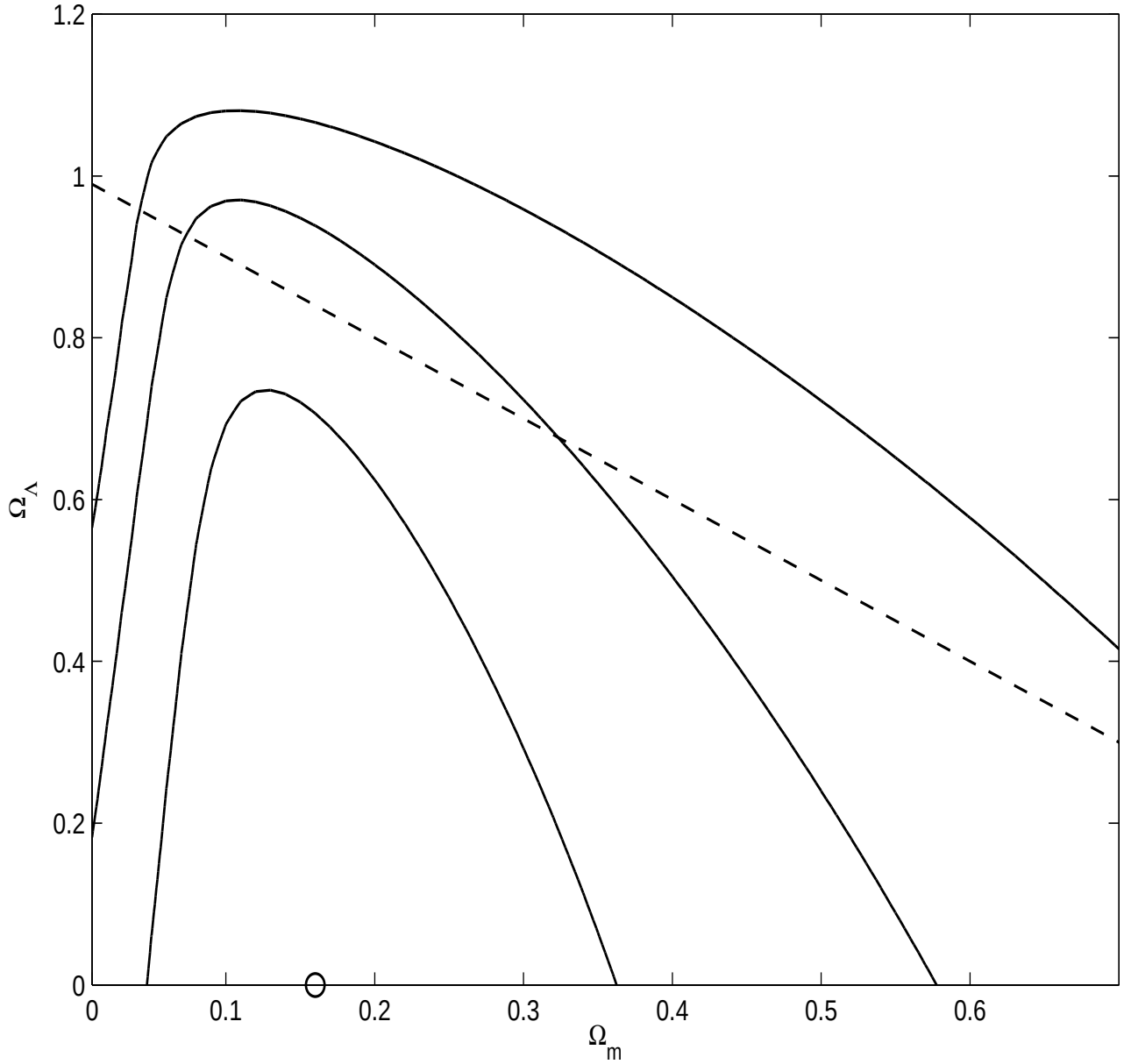

Fig. 1.— 1σ, 2σ, and 3σ confidence level contours for the ΛCDM model from the GRB data, derived using the method of Wang (2008). The circle indicates best-fit parameter values $\Omega_{\rm m} = 0.16$, $\Omega_\Lambda = 0.0$ with $\chi^2 = 0.41$ for 4 degrees of freedom. The dashed line demarcates spatially flat ΛCDM models.

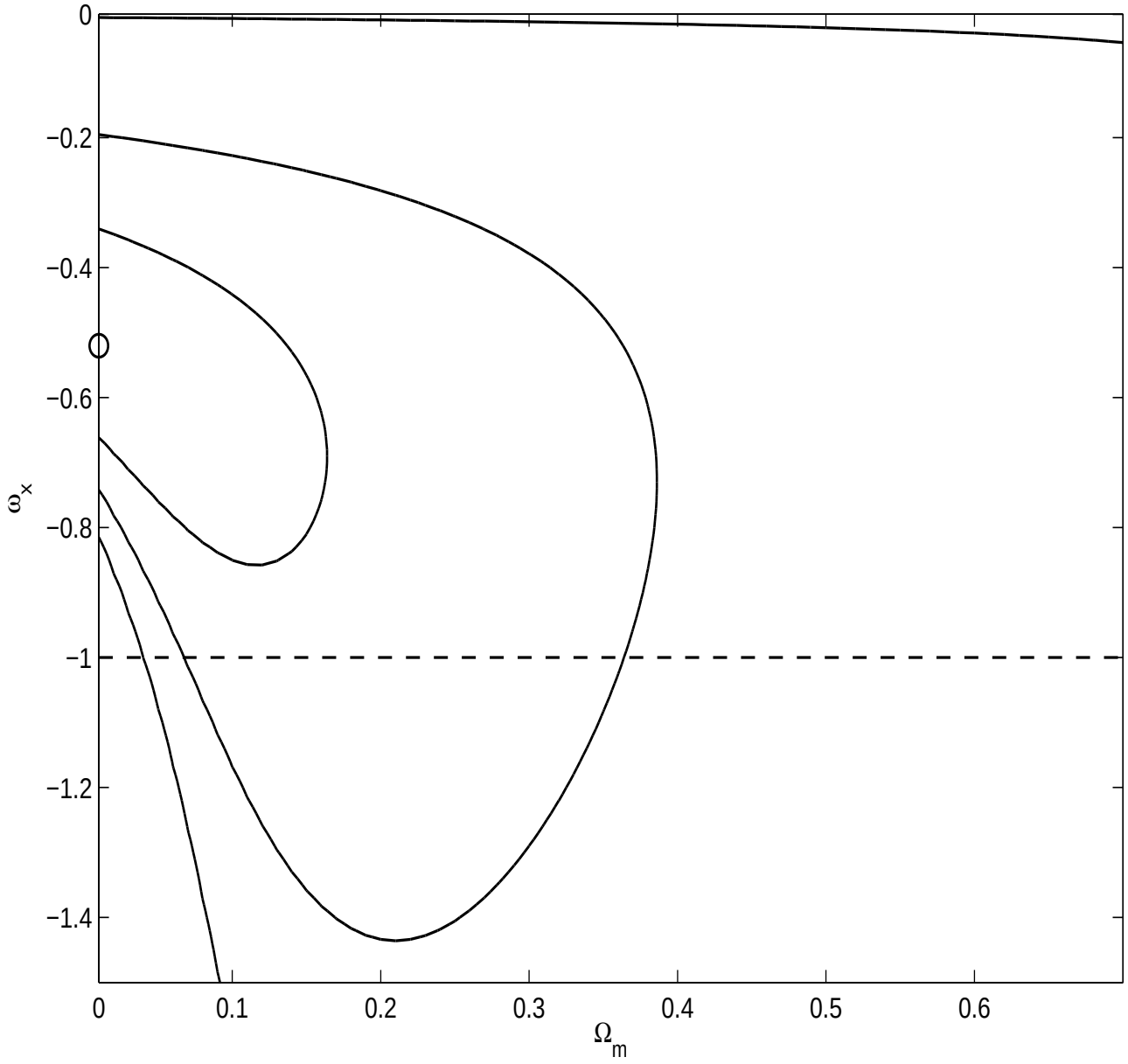

Fig. 2.— 1σ, 2σ, and 3σ confidence level contours for the XCDM model from the GRB data, derived using the method of Wang (2008). The circle indicates best-fit parameter values $\Omega_{\rm m} = 0.0$, $\omega_{\rm x} = -0.52$ with $\chi^2 = 2.17$ for 4 degrees of freedom. The dashed line demarcates spatially flat ΛCDM models.

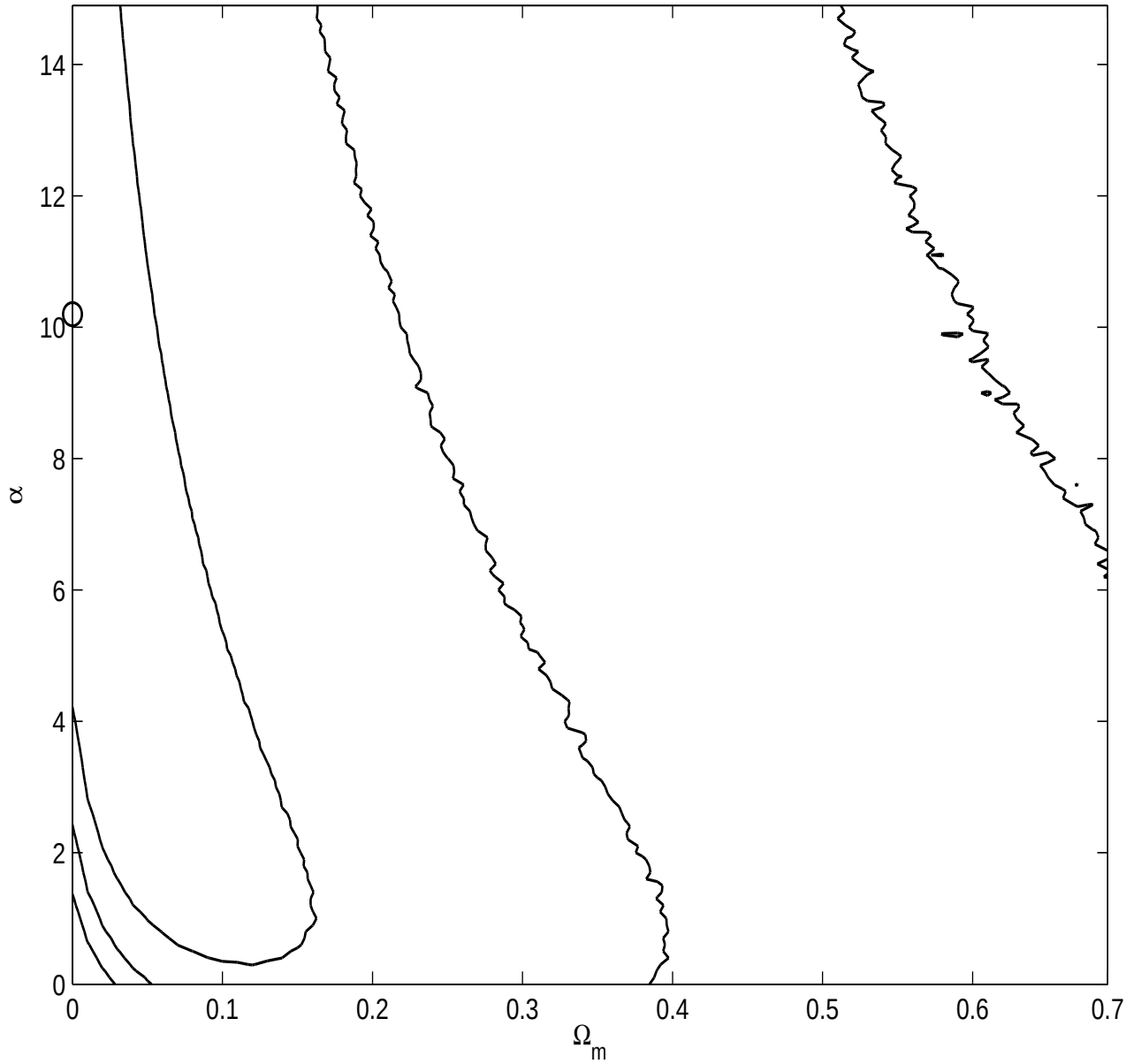

Fig. 3.— 1σ, 2σ, and 3σ confidence level contours for the ϕCDM model from the GRB data, derived using the method of Wang (2008). Numerical noise is responsible for the jaggedness of some parts of contours. The circle indicates best-fit parameter values $\Omega_{\rm m} = 0.0$, $\alpha = 10.2$ with $\chi^2 = 1.39$ for 4 degrees of freedom. The $\alpha = 0$ horizontal axis corresponds to the spatially flat ΛCDM case.

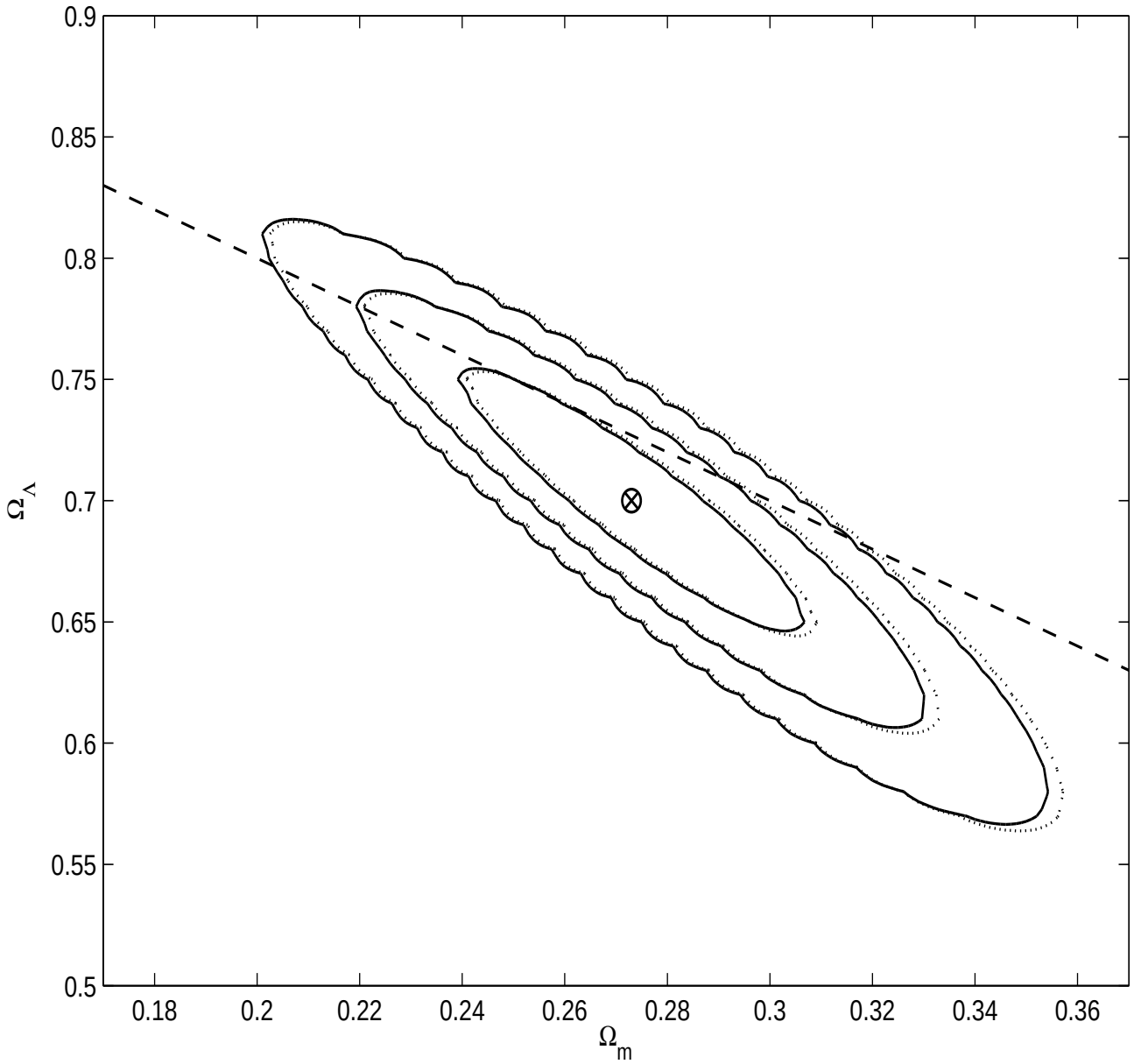

Fig. 4.— 1σ, 2σ, and 3σ confidence level contours for the ΛCDM model (dashed line demarcates spatially flat models). Solid lines (circle denotes the best-fit point) are derived using the GRB data (method of (Wang 2008)), SNe Ia Union data, and BAO peak measurements, while dotted lines (cross denotes the best-fit point) are derived using SNeIa and BAO data only. Numerical noise is responsible for the jaggedness of some parts of contours. The best-fit parameters in both cases are $\Omega_{\rm m} = 0.27$, $\Omega_\Lambda = 0.7$ with $\chi^2 = 321$ for 307 degrees of freedom (dotted lines) and $\chi^2 = 326$ for 313 degrees of freedom (solid lines). Note the different axes scales compared to Figure 1.

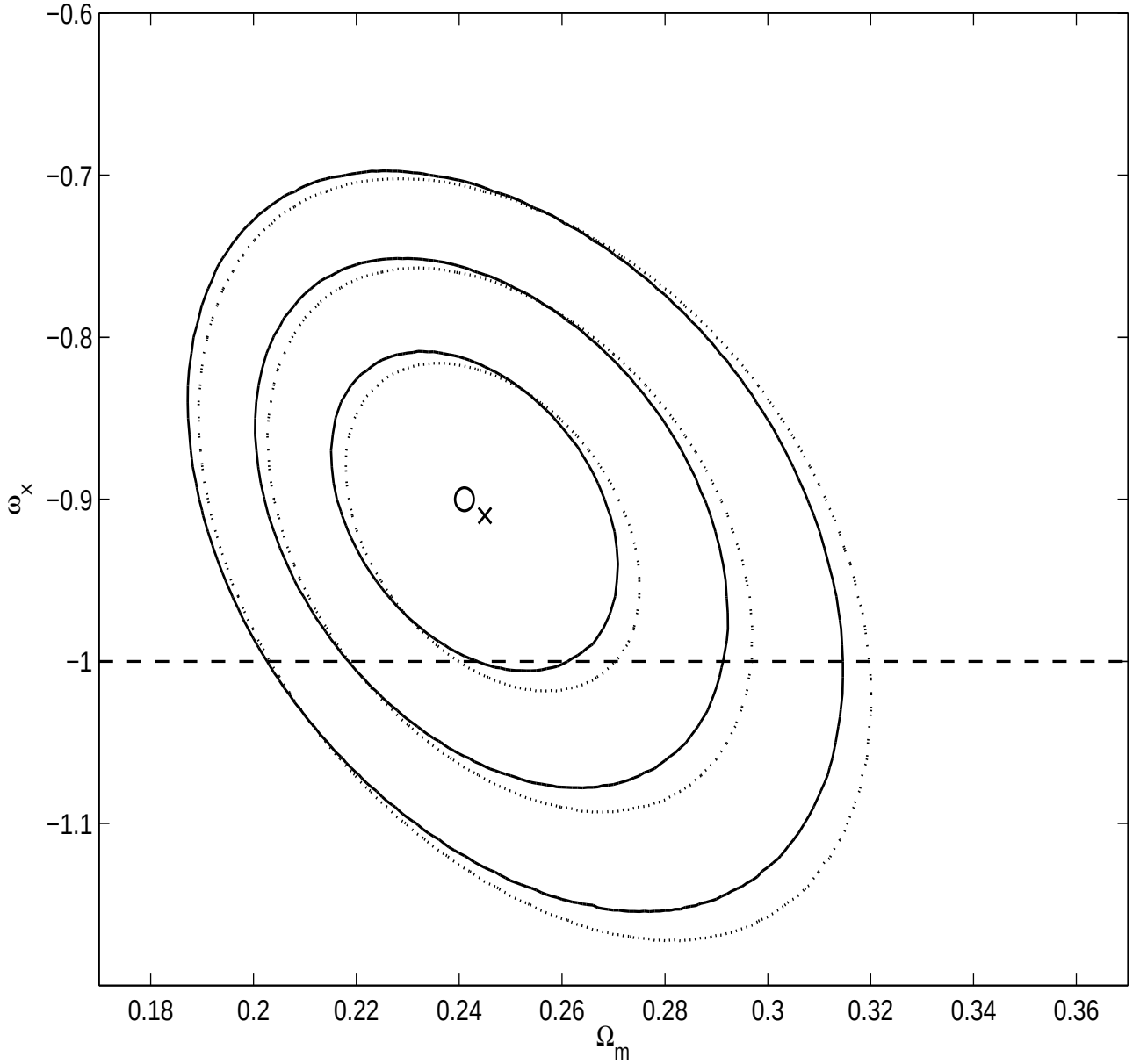

Fig. 5.— 1σ, 2σ, and 3σ confidence level contours for the XCDM model. Solid lines (circle denotes the best-fit point) are derived using GRB data (method of (Wang 2008)), SNe Ia Union data, and BAO peak measurements, while dotted lines (cross denotes the best-fit point) are derived using only SNe Ia and BAO peak data only. The best-fit parameter values are: for solid contours (circle) – $\Omega_{\rm m} = 0.24$, $\omega_{\rm x} = -0.90$ with $\chi^2 = 327$ for 313 degrees of freedom, and for dotted contours (cross) – $\Omega_{\rm m} = 0.25$, $\omega_{\rm x} = -0.91$ with $\chi^2 = 322$ for 307 degrees of freedom. Note the different axex scales compared to Figure 2.

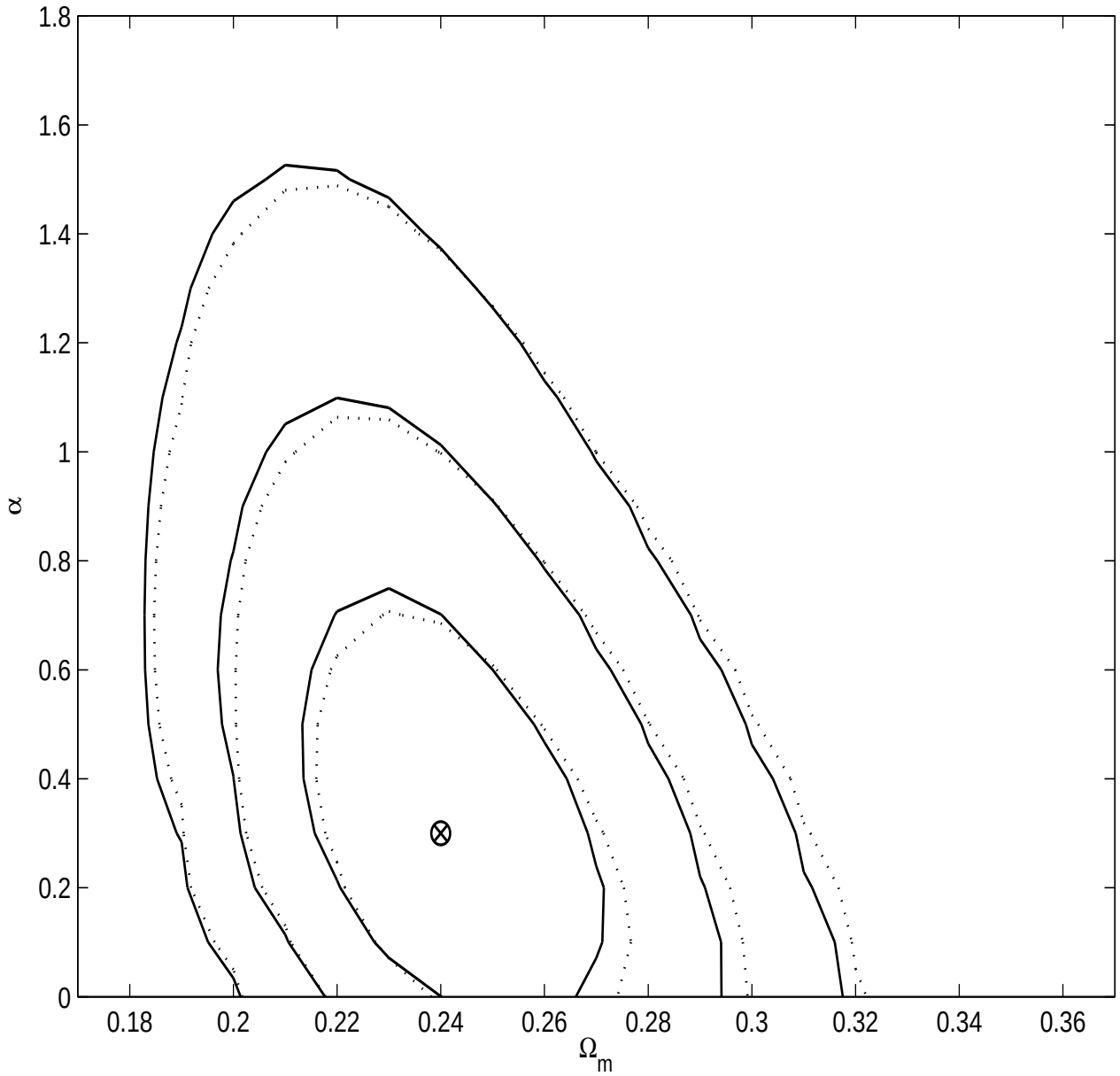

Fig. 6.— 1σ, 2σ, and 3σ confidence level contours for the ϕCDM model. Solid lines (circle denotes best-fit point) are derived using GRB data (method of (Wang 2008)), SNe Ia Union data, and BAO peak measurements, while dotted lines (cross denotes best-fit point) are derived using SNe Ia and BAO data only. Numerical noise is responsible for the jaggedness of some parts of contours. The best-fit parameters in both cases are: $\Omega_{\rm m} = 0.24$, $\alpha = 0.30$ with $\chi^2 = 326$ for 313 degrees of freedom (solid lines) and $\chi^2 = 321$ for 307 degrees of freedom (dotted lines). Note the different axes scales compared to Figure 3.

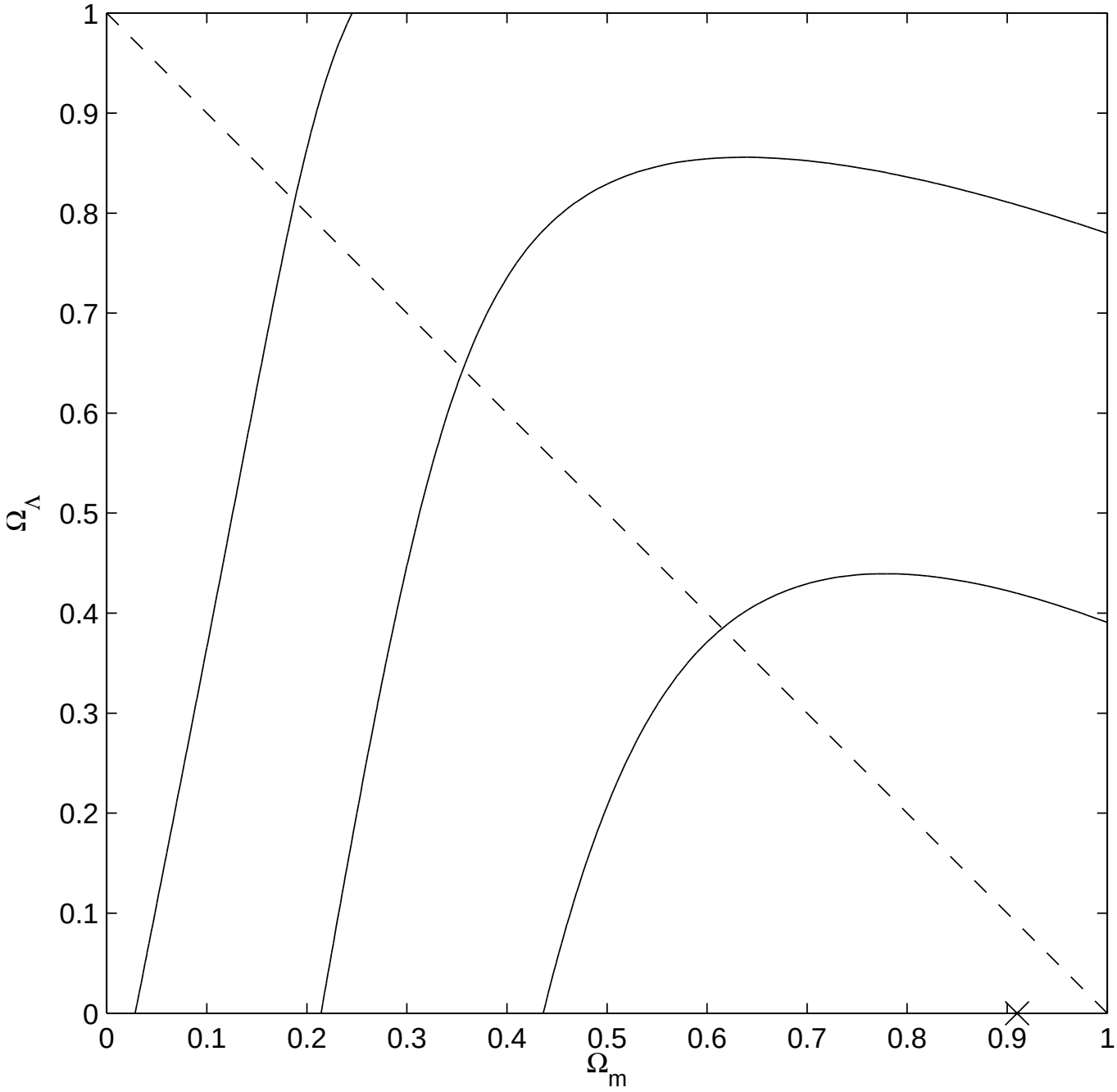

Fig. 7.— 1σ, 2σ, and 3σ confidence level contours for the ΛCDM model from the GRB data, derived using the method of Schaefer (2007). The cross indicates best-fit parameter values $\Omega_{\rm m} = 0.91$, $\Omega_\Lambda = 0.0$ with $\chi^2 = 77.86$ for 67 degrees of freedom. The dashed line demarcates spatially flat ΛCDM models.

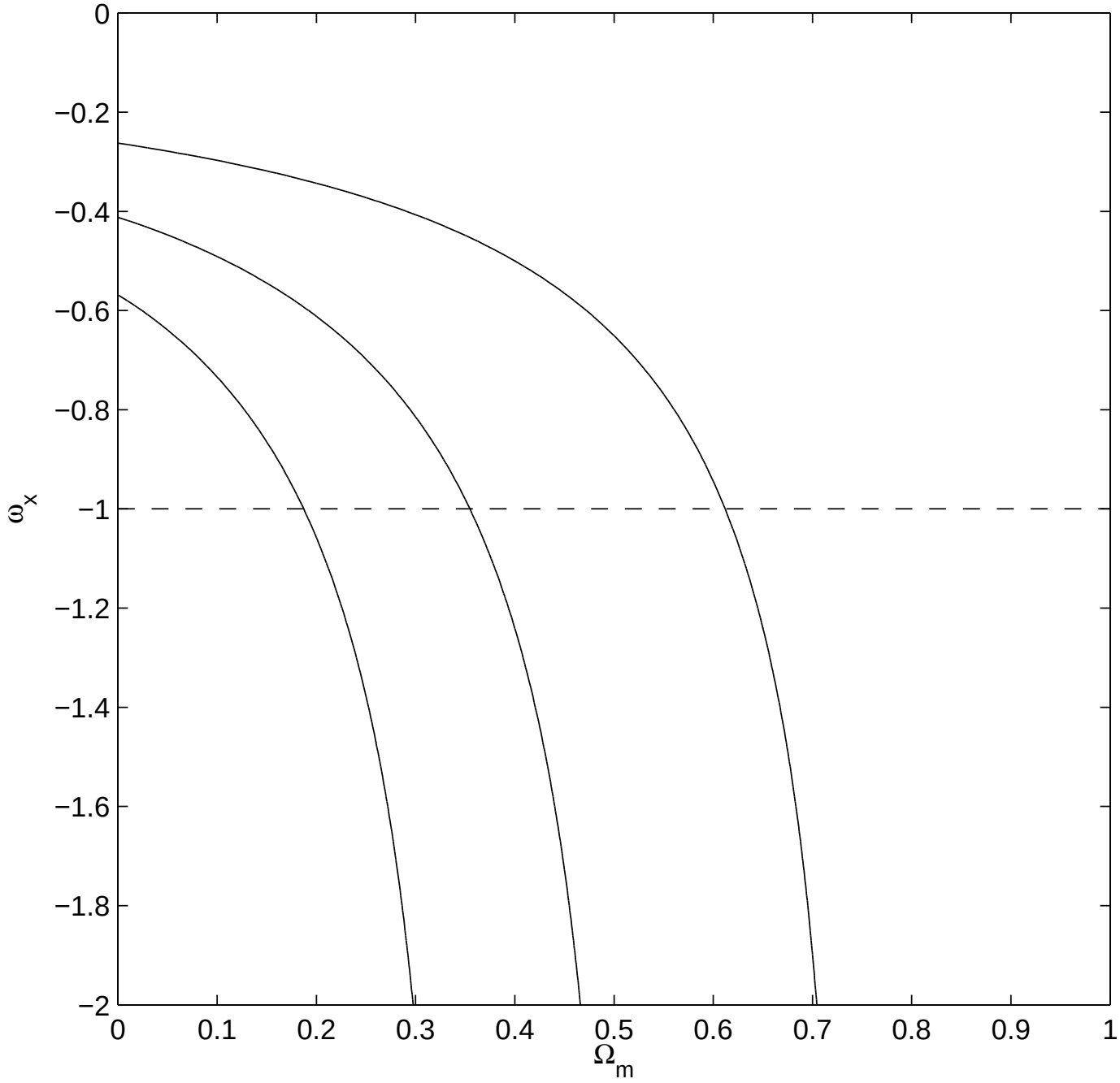

Fig. 8.— 1σ, 2σ, and 3σ confidence level contours for the XCDM model from the GRB data, derived using the method of Schaefer (2007). The best fit is achieved on the line $\omega_{\rm x} = 0.00$, which corresponds to the spatially flat matter-dominated Universe, $\chi^2 = 77.8$ for 67 degrees of freedom. The dashed line demarcates spatially flat ΛCDM models.

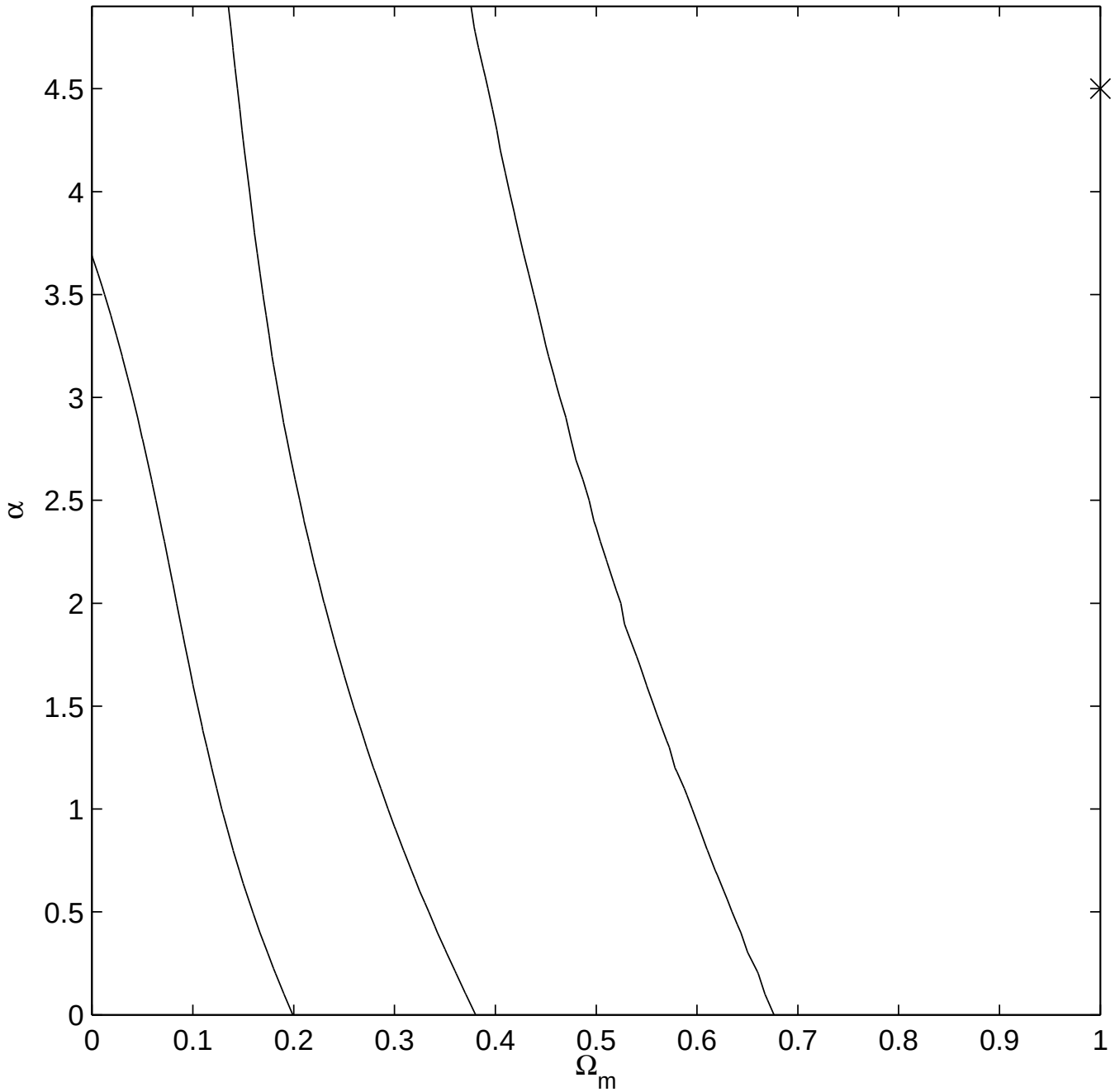

Fig. 9.— 1σ, 2σ, and 3σ confidence level contours for the ϕCDM model from the GRB data, derived using the method of Schaefer (2007). The cross indicates best-fit parameter values $\Omega_{\rm m} = 1.0$, $\alpha = 4.5$ with $\chi^2 = 77.8$ for 67 degrees of freedom. The $\alpha = 0$ horizontal axis corresponds to the spatially flat ΛCDM case.

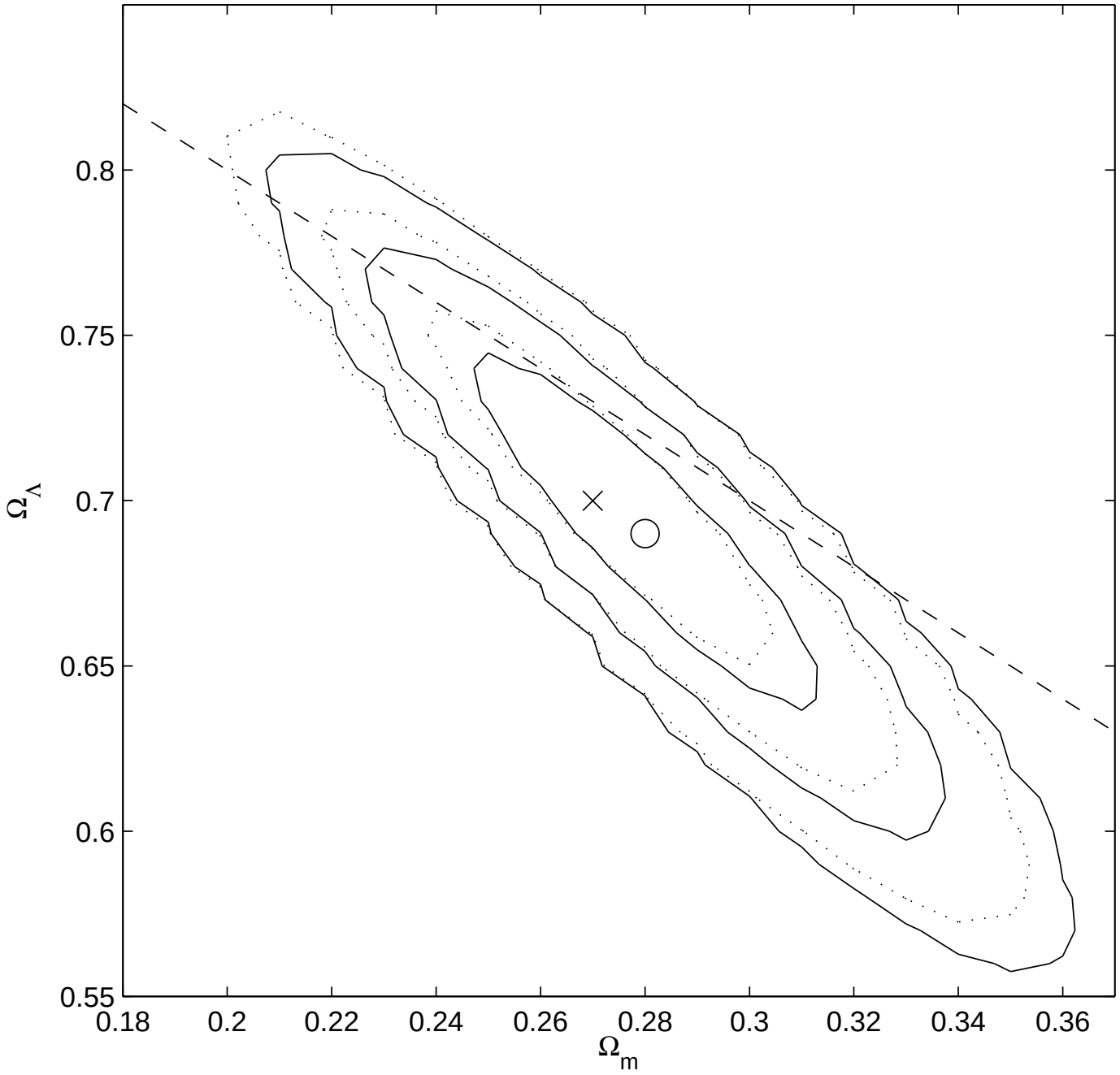

Fig. 10.— 1σ, 2σ, and 3σ confidence level contours for the ΛCDM model (dashed line demarcates spatially flat models). Solid lines (circle denotes the best-fit point) are derived using the GRB data (method of (Schaefer 2007)), SNe Ia Union data, and BAO peak measurements, while dotted lines (cross denotes the best-fit point) are derived using SNe Ia and BAO data only. Numerical noise is responsible for the jaggedness of some parts of the contours. The best-fit parameters are $\Omega_m = 0.27$, $\Omega_\Lambda = 0.7$ with $\chi^2 = 321$ for 307 degrees of freedom (dotted lines) and $\Omega_m = 0.28$, $\Omega_\Lambda = 0.69$ with $\chi^2 = 401$ for 376 degrees of freedom (solid lines). Note the different axes scales compared to Figure 7.

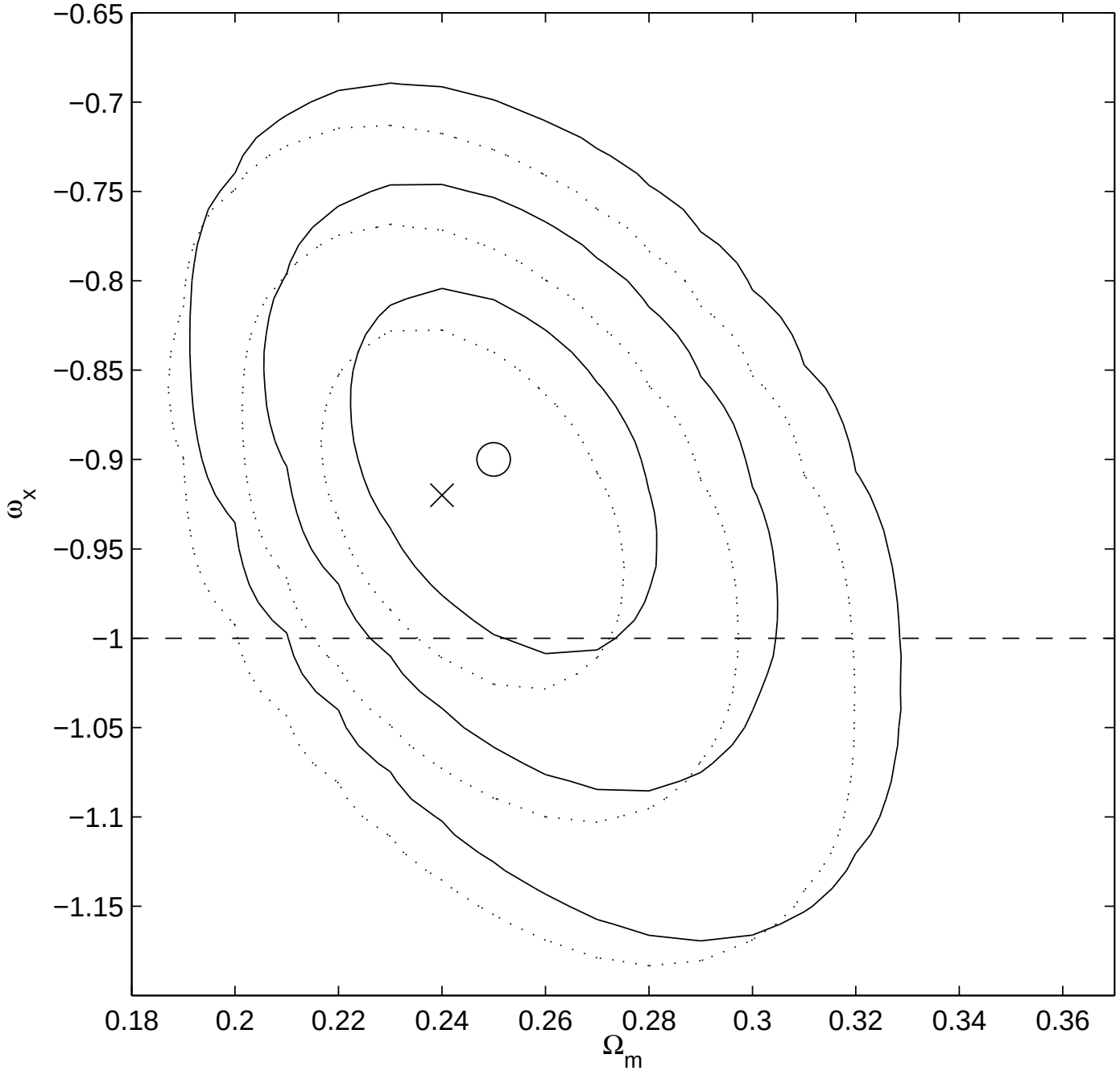

Fig. 11.— 1σ, 2σ, and 3σ confidence level contours for the XCDM model. Solid lines (circle denotes the best-fit point) are derived using GRB data (method of (Schaefer 2007)), SNe Ia Union data, and BAO peak measurements, while dotted lines (cross denotes the best-fit point) are derived using SNe Ia and BAO peak data only. The best-fit parameter values are, for solid contours (circle) – $\Omega_{\rm m} = 0.26$, $\omega_{\rm x} = -0.90$ with $\chi^2 = 401$ for 376 degrees of freedom, and for dotted contours (cross) – $\Omega_{\rm m} = 0.25$, $\omega_{\rm x} = -0.91$ with $\chi^2 = 322$ for 307 degrees of freedom. Note the different axes scales compared to Figure 8.

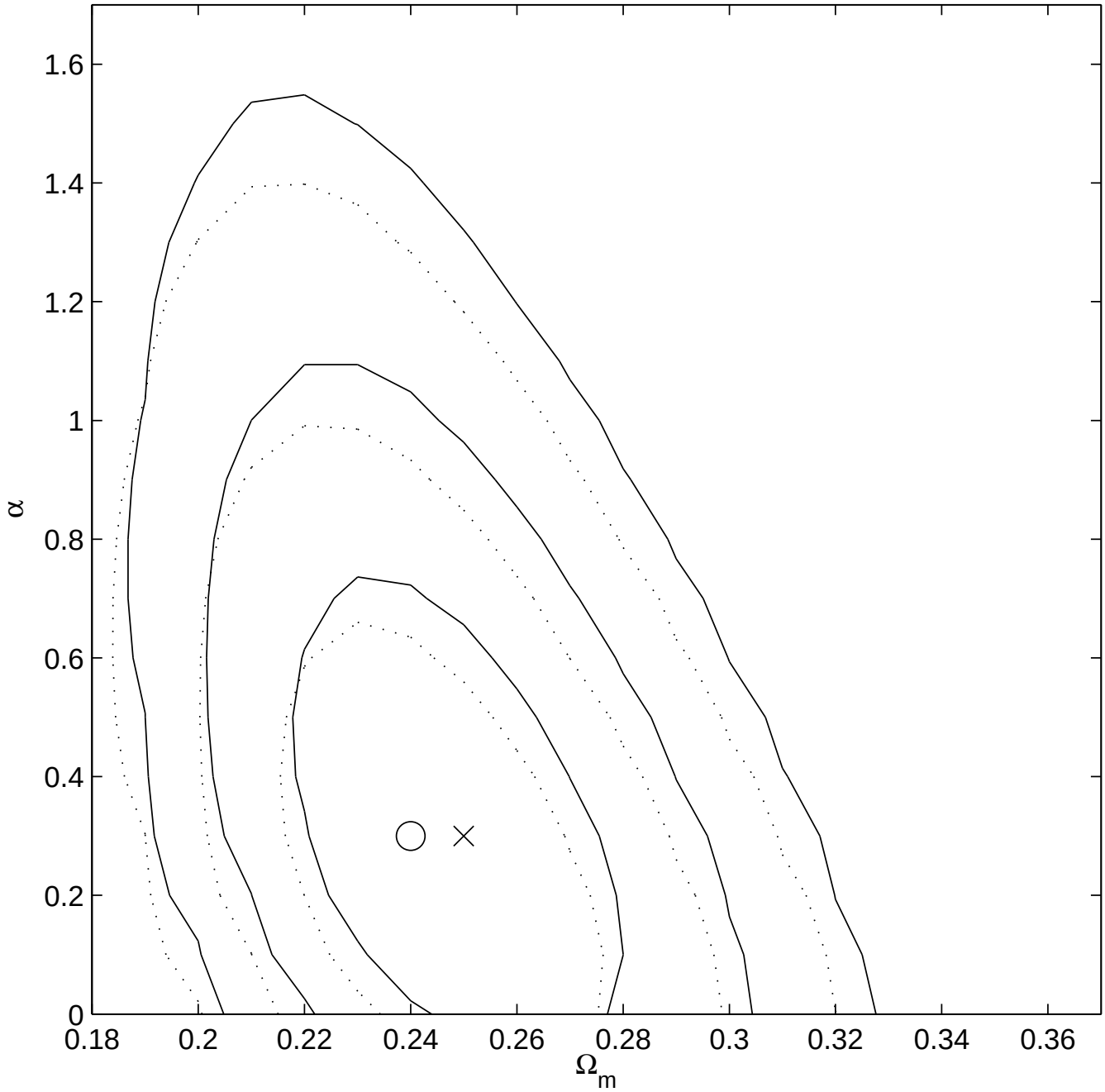

Fig. 12.— 1σ, 2σ, and 3σ confidence level contours for the ϕCDM model. Solid lines (circle denotes best-fit point) are derived using GRB data (method of (Schaefer 2007)), SNe Ia Union data, and BAO peak measurements, while dotted lines (cross denotes best-fit point) are derived using SNe Ia and BAO data only. The best-fit parameters are $\Omega_{\rm m} = 0.24$, $\alpha = 0.30$ with $\chi^2 = 401$ for 376 degrees of freedom (solid lines) and $\Omega_{\rm m} = 0.25$, $\alpha = 0.30$ with $\chi^2 = 321$ for 307 degrees of freesom (dotted lines). Note different axes scales compared to Figure 9.